Optics Communications 380 (2016) 161–167

Contents lists available at ScienceDirect

Optics Communications

journal homepage: www.elsevier.com/locate/optcom

Freeform lens collimating spectrum-folded Hadamard transform near-infrared spectrometer

Xiaoduo Wang [a,*], Hua Liu [b], Larissa Juschkin [c], Yunpeng Li [d], Jialin Xu [b], Xiangqian Quan [b,e], Zhenwu Lu [b]

[a] Shenyang Institute of Automation, Chinese Academy of Sciences, Shenyang 110016, China
[b] Changchun Institute of Optics, Fine Mechanics and Physics, Chinese Academy of Sciences, Changchun 130033, China
[c] RWTH Aachen University, Aachen 52074, Germany
[d] National Police University of China, Shenyang 110000, China
[e] University of Chinese Academy of Sciences, Beijing 100049, China

ARTICLE INFO

Article history:
Received 3 March 2016
Received in revised form
12 May 2016
Accepted 3 June 2016

Keywords:
Near-infrared Spectrometer
Hadamard transform
Freeform surface
Digital micro-mirror devices
Grating

ABSTRACT

A novel Hadamard transform spectrometer collimated by a freeform lens has been designed, which doubles the working spectral range while the spectral resolution is maintained. The freeform lens is designed to redistribute the broadband spectra of the source from 800 nm to 2400 nm into two collimated beams with different wavelengths and different tilting angles, to achieve the folding of spectra on the digital micro-mirror devices (DMD). It is constructed by solving two partial differential equations. The grating diffraction efficiency of the two split beams are more uniform and higher compared with the traditional method. The simulation results show that the bandwidth of the spectrometer is doubled and the spectral resolution is better than 10 nm. The optical system becomes more compact, and the energy efficiency is improved by 11.98% by folding the spectra with one freeform lens and one grating.

1. Introduction

Near-infrared spectroscopy is becoming a well-established analytical method to achieve quality monitoring and product analysis in a wide range of applications ranging from agriculture to petrochemical industry and also clinical medicine areas [1–3]. In many cases, it's important to measure the spectra with high resolution and wide working wavelength range. For example, to identify the quality of milk powder or medicinal material, a spectrometer which has a wavelength range of 800–2500 nm with a resolution better than 10 nm is necessary to make the measurement accurately and precisely [4]. However, most of the commercially available near-infrared spectrometers can't achieve high resolution and wide working wavelength range at the same time, such as AvaSpec-NIR256-2.2 which has a spectral resolution of 15 nm at working wavelength range of 1000–2200 nm. This kind of situation has hindered the widespread use of portable near-infrared spectrometer.

In a previous publication [5], we doubled the working wavelength range of a portable Hadamard transform spectrometer (HTS) with no decrease of the spectral resolution by using two sub-gratings tilting with different angles. The spectral resolution was 5.5 nm while the working wavelength range was from 800 nm to 2000 nm. However, in its practical implementation, there are some limitations with respect to the stray light caused by the two sub-gratings and the precision of the sub-grating integration, especially when the number of sub-gratings increases to several tens [6]. Based on those findings, we propose a novel optical system which not only reduces the complexity of the spectrometer, but also improves the optical performance.

Compared with traditional optical components, freeform optics can precisely control the distribution of light beams, and simplify the system with fewer surfaces, lower mass which reduces the difficulty in assembly [7–10]. In this study, we propose a novel source collimating approach by using freeform lens to extend the working wavelength range. The freeform lens is designed to redistribute the light from source into two collimated beams in different directions with different wavelength regions, from 800 nm to 1600 nm and from 1600 nm to 2400 nm, respectively. Then only one plane grating is used to fold the spectra on DMD. The main contribution of this article is presented in Section 2: the derivation of the incident angles of the two collimated beams and the calculation and construction of the freeform surface. The diffraction efficiency of the grating is optimized to be more uniform and higher over the entire band. The optical layout and simulation

* Corresponding author at: Shenyang Institute of Automation, Chinese Academy of Sciences, Shenyang 110016, China.
E-mail address: wangxdsxs@yeah.net (X. Wang).

http://dx.doi.org/10.1016/j.optcom.2016.06.009
0030-4018/

results are showed in Section 3. By folding the two bands on DMD, the working spectrum range of the spectrometer is doubled while the resolution is maintained. The spectral resolution is better than 10 nm and the diameter of the single element detector is smaller than 4 mm. The simulation results show that the optical system of this spectrometer becomes more compact, and the energy efficiency is improved by 11.98%. What's more, the secondary spectra of the spectrum-folded spectrometer are much easier to be eliminated compared with traditional broadband spectrometers.

2. Design method of novel source collimating approach

2.1. The derivation of the incident angles

As an improvement, here a freeform lens is designed to redistribute the irradiance from optical fiber into two collimated beams in different directions propagating towards the grating, as shown in Fig. 1. Then the two dispersed beams are focused onto the DMD by imaging lens, folding the entire working spectrum into two parallel and aligned spectral stripes on DMD with only one grating. The DMD composed of a micro-mirror array of 1024×768, and each mirror rotates either $+12^\circ$ or -12° axis to the diagonal line according to the code of Hadamard matrix [11]. It is used as the mask of Hadamard transform to implement the spectrum encoding. The modulated spectrum are reflected by DMD and focused by the converging lens onto a single element detector. The original spectra of the source are acquired by the decoding of Hadamard transform [12].

In this work, the working spectra of the HTS, λ_1 to λ_3, is divided into two bands with equal bandwidth of the wavelength window, λ_1 to λ_2 (band A) and λ_2 to λ_3 (band B), corresponding to the two spectral columns folded on DMD respectively. The incidence angles onto the plane grating are the same for all the wavelengths of band A, so as band B. The grating equation yields:

$$\sin \delta_{\mathrm{Amax}} - \sin \delta_{\mathrm{Amin}} = \frac{m(\lambda_2 - \lambda_1)}{d} = \frac{m\Delta\lambda}{d}, \tag{1}$$

$$\sin \delta_{\mathrm{Bmax}} - \sin \delta_{\mathrm{Bmin}} = \frac{m(\lambda_3 - \lambda_2)}{d} = \frac{m\Delta\lambda}{d}, \tag{2}$$

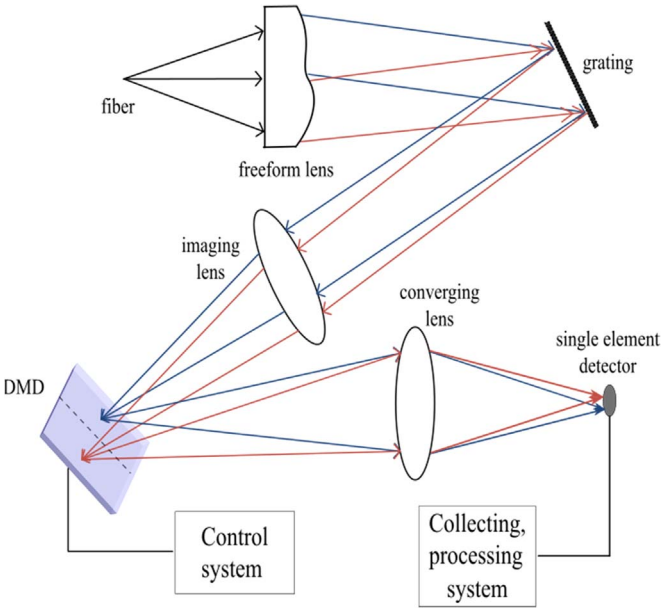

Fig. 1. Schematic layout of the spectrum-folded near-infrared HTS.

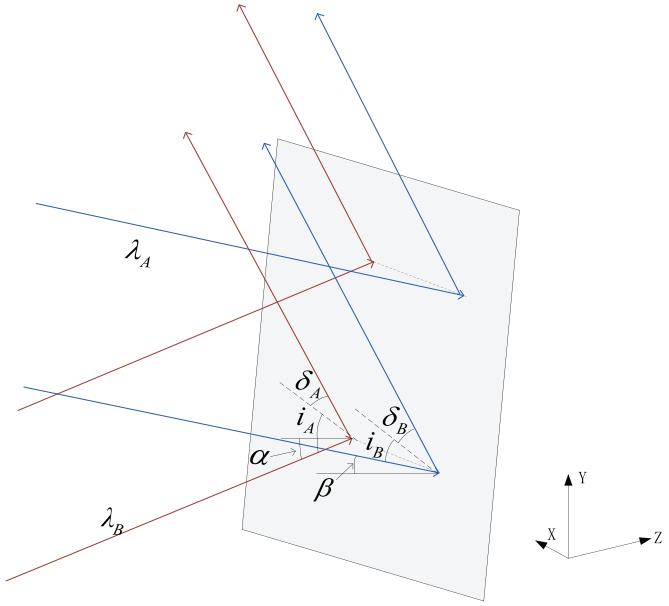

Fig. 2. Schematic of the light diffraction of bands A and B on the grating.

where δ_{Amax}, δ_{Amin} , δ_{Bmax}, δ_{Bmin} are the maximum and minimum diffraction angles of spectra in band A and B, respectively. m is the order of diffraction and d is the groove space of the grating. From Eqs. (1) and (2), it can be concluded that the spectra of band A and B are distributed within the same range of the diffraction angles when the value of m and d is specified.

After being collimated by the freeform lens, rays of band A and band B are incident on the grating with different angles i_{A} and i_{B}, as shown in Fig. 2. δ_{A} and δ_{B} are the diffraction angles of λ_{A} and λ_{B}, which are the corresponding central wavelengths of band A and B, respectively. α is the angle between the collimated beam of band A and Z axis. β is the angle between the collimated beam of band B and Z axis. Z axis is the optical axis of the system. In order to align the corresponding spectra of the two bands on the DMD surface, their diffraction angles should be the same, which means $\delta_{\mathrm{A}}=\delta_{\mathrm{B}}$. Then the relationship between the incidence angles and the wavelengths can be derived as:

$$\sin i_{\mathrm{A}} - \sin i_{\mathrm{B}} = \frac{m(\lambda_{\mathrm{A}} - \lambda_{\mathrm{B}})}{d}. \tag{3}$$

According to Eq. (3), the value of i_{A} can be calculated once the value of i_{B} is specified, and vice versa. When the angle between the grating normal and the Z axis is specified, the tilt angles of the two collimated beams can be derived, which are essential to the ray tailoring calculation of the freeform surface.

2.2. Calculation and construction of the freeform lens

To simplify the mathematical model, two assumptions are made: (1) the front surface of the freeform lens is spherical and centered at the origin of the coordinate; (2) a point source located at the center of the sphere is adopted as the source. A ray sent out from the source is incident on the front surface perpendicularly and intersects with the freeform surface at point P. The coordinate of point $P(P_x, P_y, P_z)$ can also be expressed as $P(\rho(\theta, \varphi), \theta, \varphi)$ in the spherical coordinate system. The ray from point P strikes the grating at point $G(x, y, z)$. Fig. 3 illustrates how a ray from the point source is uniquely tailored to a point on the grating plane. $\boldsymbol{I}$, $\boldsymbol{O}$ and $\boldsymbol{N}$ are the incident, refractive and normal unit vectors at point P, respectively. They can be expressed as: $\boldsymbol{I} = (I_x\boldsymbol{e}_x, I_y\boldsymbol{e}_y, I_z\boldsymbol{e}_z) = (\sin\varphi\cos\theta\boldsymbol{e}_x, \sin\varphi\sin\theta\boldsymbol{e}_y, \cos\varphi\boldsymbol{e}_z)$ and

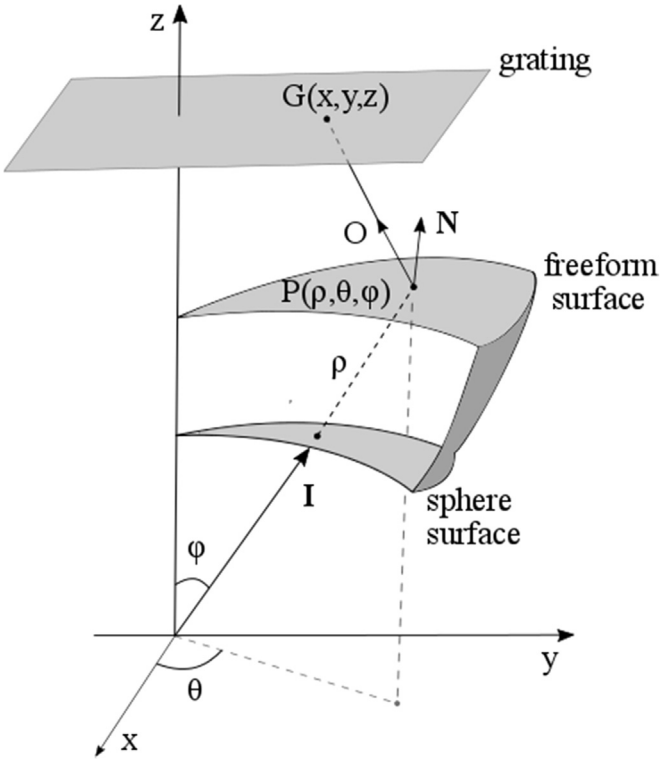

Fig. 3. The geometric layout of the freeform lens.

$\boldsymbol{O}=(O_x\boldsymbol{e}_x, O_y\boldsymbol{e}_y, O_z\boldsymbol{e}_z)$. According to the vector form of Snell's law [13], the following two partial differential equations [14] can be derived:

$$\begin{cases} \rho_\varphi = \rho\dfrac{\sin\varphi(O_z - nI_z) - \cos\varphi\left[\cos\theta(O_x - nI_x) + \sin\theta(O_y - nI_y)\right]}{\cos\varphi(O_z - nI_z) + \sin\varphi\left[\cos\theta(O_x - nI_x) + \sin\theta(O_y - nI_y)\right]} \\ \rho_\theta = \rho\sin\varphi\dfrac{\sin\theta(O_x - nI_x) - \cos\theta(O_y - nI_y)}{\cos\varphi(O_z - nI_z) + \sin\varphi\left[\cos\theta(O_x - nI_x) + \sin\theta(O_y - nI_y)\right]} \end{cases}, \tag{4}$$

where n is the refractive index of the freeform lens, ρ_θ and ρ_ϕ are the first-order partial derivatives of ρ with respect to θ and ϕ. Once the three components of vector $\boldsymbol{O}$ are acquired, the sampling points of the freeform surface can be obtained by solving the partial differential equations above.

To fold the two spectral bands on the surface of DMD, the freeform surface is designed to split the diverging beam from the point source into two collimated beams tilted at different angles with respect to the optical axis (Z axis) as mentioned in Section 2.1. If both bands A and B are tilted only in YZ plane, the spectra of band A and B will overlap with each other on the DMD. To avoid this situation, at least one of the collimated beams should tilt in XZ plane with a small angle. In our work, beam B is collimated by the lower part (the value of y coordinate of point P is smaller than zero) of the freeform lens and is tilted both in YZ and XZ plane at angles of α and γ, respectively. Beam A is collimated by the upper part (the value of y coordinate of point P is bigger than zero) of the freeform lens and is tilted only in YZ plane at an angle β. Then the vector $\boldsymbol{PG}$ of the upper part and lower part of the lens can be computed as:

$$\boldsymbol{PG}_{\text{upper}} = (0, (z - P_z)\tan\beta, z - P_z), \tag{5}$$

$$\boldsymbol{PG}_{\text{lower}} = ((z - P_z)\tan\gamma, (z - P_z)\tan\alpha, z - P_z), \tag{6}$$

where z is the distance between the point source and the grating. The unit vectors of the upper and lower part outgoing rays from the freeform lens are derived as:

$$\boldsymbol{o}_{\text{upper}} = \left(0, \frac{\tan\beta}{\sqrt{1+\tan^2\beta}}, \frac{1}{\sqrt{1+\tan^2\beta}}\right), \tag{7}$$

$$\boldsymbol{o}_{\text{lower}} = \left(\frac{\tan\gamma}{\sqrt{1+\tan^2\gamma+\tan^2\alpha}}, \frac{\tan\alpha}{\sqrt{1+\tan^2\gamma+\tan^2\alpha}}, \frac{1}{\sqrt{1+\tan^2\gamma+\tan^2\alpha}}\right), \tag{8}$$

Points P and G are related through geometrical-optics approach, which is different from the energy conservation based tailoring method generally used in freeform surface design for illumination and reshaping applications.

Substituting Eq. (7) or Eq. (8) into Eq. (4), ρ_θ and ρ_ϕ become functions of $\rho(\theta, \phi, \gamma)$. In this work, γ is set to be 3°, ϕ varies from 0° to 12°. Considering that the partial differential equations for bands A and B are different, the sampling points for the upper and lower parts of the freeform lens are calculated separately, so θ varies from 0° to 180° and from 180° to 360° for the upper and lower parts freeform lens, respectively. The material of the lens is set to be N-BK7. The contour of the freeform surface is constructed by solving the partial nonlinear differential equations. Since the exact solution of the partial differential equations is difficult or not at all to get, the fourth order Runge-Kutta method is used to obtain the numerical solution. The starting point is set to be (0, 0, 35 mm), which is the intersection of the freeform surface with the Z axis.

Fig. 4 shows the discrete sampling points of the upper and lower parts of the surface when $\alpha=-6.11°$ and $\beta=8.03°$, and positive angles are defined for counterclockwise rotation and negative angles for clockwise rotation. The calculation takes about 20 s by a computer with 2 GHz CPU. So it's time efficient to get a freeform lens through this approach. The smooth freeform surface is constructed with non-uniform rational B-splines (NURBS) in CAD software, as presented in Fig. 5. From Fig. 5, it can be found that there's a dislocation at the intersection of the two parts, which is resulted from the tilting of the lower part in XOZ plane. To fold the two spectra stripes without overlapping, this is more or less inevitable, depending on the value of γ. Meanwhile, the advanced manufacturing technology makes it feasible to fabricate such a freeform surface, either by injection casting, ion implantation and flying cut with high performance at present [15–17].

3. Parameters and simulation result

The numerical aperture of the fiber is 0.2. A 0.7 XGA DMD chip with pixel size of 13.68 μm and a ±12° tilt angle is adopted. The wavelength range of band A is from 800 nm to 1600 nm and that of band B is from 1600 nm to 2400 nm. The plane grating with a groove density of 300 grooves/mm is tilted at 13.89° in YZ plane. The incidence angles of bands A and B are 20° and 5.86° in YZ plane, respectively. The minimal diffraction efficiency of the grating for spectra of band A and B is higher than 67% and 78%, respectively, as shown in Fig. 6. However, the minimal diffraction efficiency of the grating reduces to 35% when the whole spectrum incident on the grating with the same angle of 13.89°. From Fig. 6, we can see that the diffraction efficiency is more uniform and higher over the entire band because of the beam splitting. The radius of the spherical surface in the freeform lens is 30 mm, and the focal length of the imaging lens is 35 mm. The theoretical resolution is 5.5 nm, when the diameter of the fiber is 100 μm. Considering that the distance between the source and the freeform surface is much larger than the size of the source, the fiber here can be regarded as a point source, so it has little influence on the performance of the freeform lens.

A side view of the optical system simulated by optical design software Zemax is shown in Fig. 7. The spot diagrams of bands A

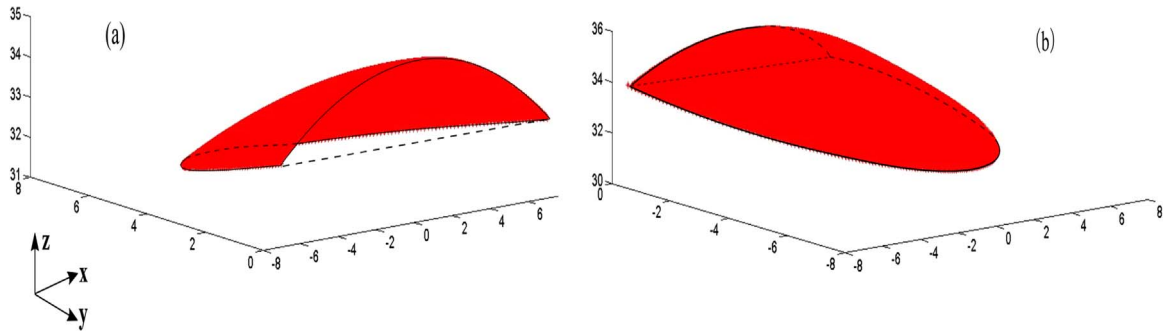

Fig. 4. The discrete sampling points of the lower (a) and upper (b) part of the freeform surface obtained by computing. The number of sampling points is 500 × 1000 for each part.

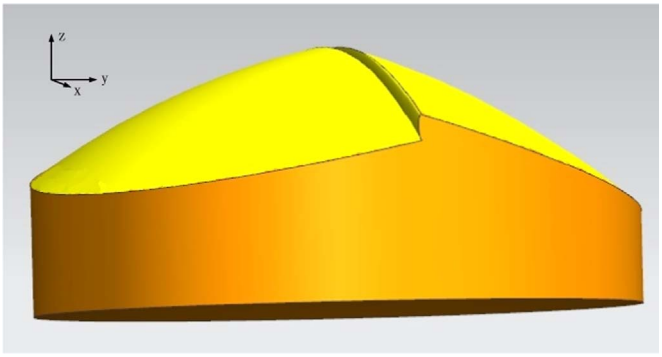

Fig. 5. The freeform lens constructed in CAD software.

and B on the grating after being collimated by the freeform surface are shown in Fig. 8(a). The shapes of the two spots are in good consistence with the profiles of the ray incident on the corresponding surface part (upper and lower) of the freeform lens, which are perfect standard semicircles. It indicates high performance of beams collimation. The width of the grating is a half comparing the case of no spectrum folding, which makes the spectrometer more compact. The imaging lens is constituted of two doublet lens. From Fig. 7, it can be seen that the spectra of bands A and B are parallel, aligned and end to end on the DMD. A toroidal lens is adopted as the converging lens to focus the spot on the single element detector both in x and y directions. The focal lengths of the toroidal lens in x and y direction are 10.3 mm and 21.3 mm, respectively. The spots of different wavelengths of band A and band B focused on the detector are shown in Fig. 8(b). The diameter of the overlapped spot is smaller than 4 mm, and a 5 mm single element detector is a much more cost effective and compact solution compared to an array detector. Fig. 9 shows two sets of spot diagrams and the energy distribution of the two distinguishable wavelengths in DMD. According to Rayleigh criterion,

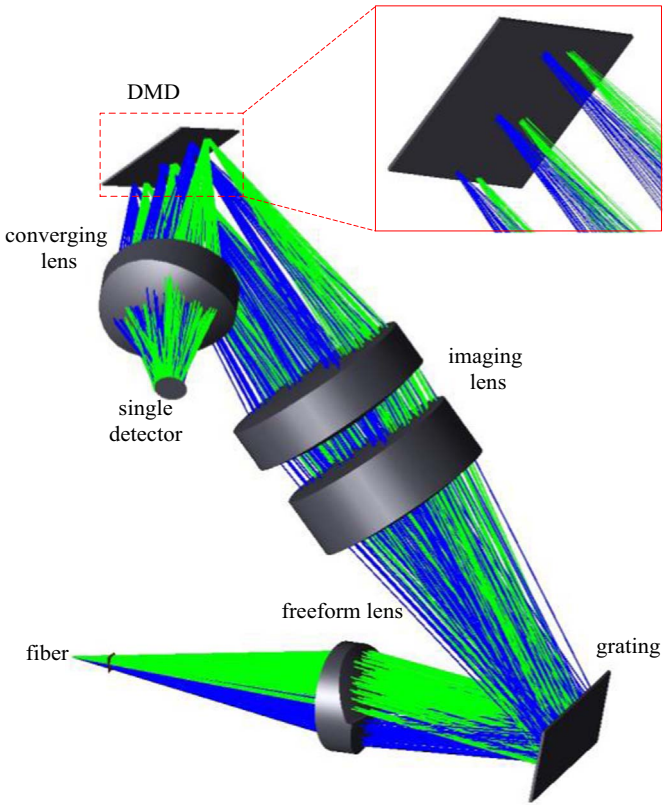

Fig. 7. Side view of the optical shaded model. The rays in blue and green color represent wavelengths of band A and B, respectively. For spectrum on DMD, from bottom to top, the green rays denote 800 nm, 1200 nm, 1600 nm, the blue rays denote 1600 nm, 2000 nm and 2400 nm. (a) Spots diagrams on grating (b) footprint on the single element detector. (For interpretation of the references to color in this figure legend, the reader is referred to the web version of this article.)

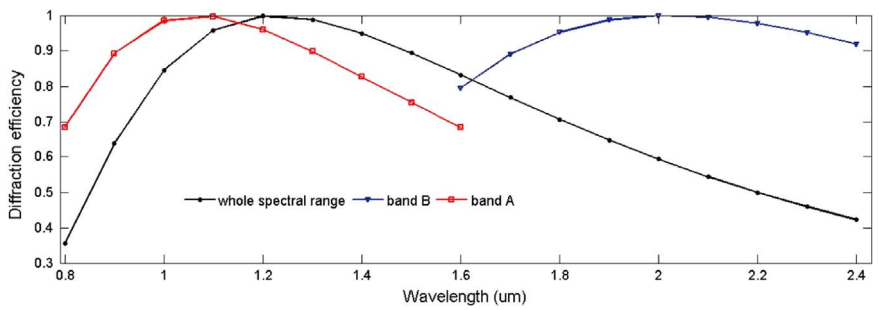

Fig. 6. Grating diffraction efficiency at different wavelengths, the incidence angle for bands A and B are 20° and 5.86°. The diffraction efficiency of the whole spectral range is calculated assuming that the ray incident parallel to the Z axis.

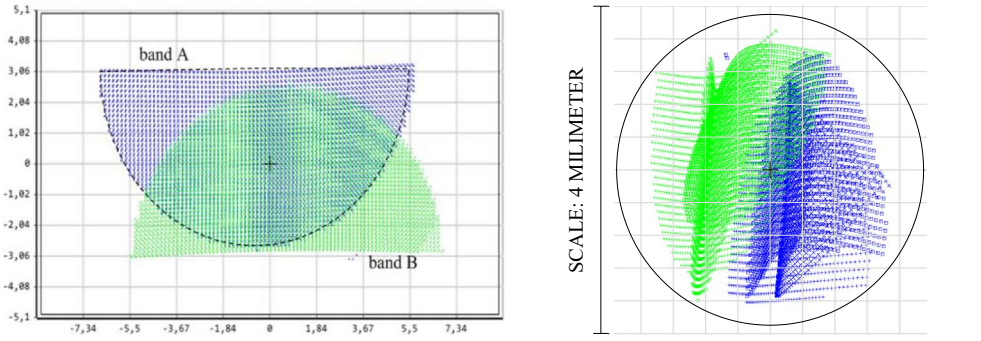

(a) Spots diagrams on grating (b) footprint on the single element detector

Fig. 8. Spots diagrams on grating (a) and single element detector (b). The dashed dark line on (a) is a standard semicircle. The blue and green color dots denote the wavelengths of band A and band B, respectively. (For interpretation of the references to color in this figure legend, the reader is referred to the web version of this article.)

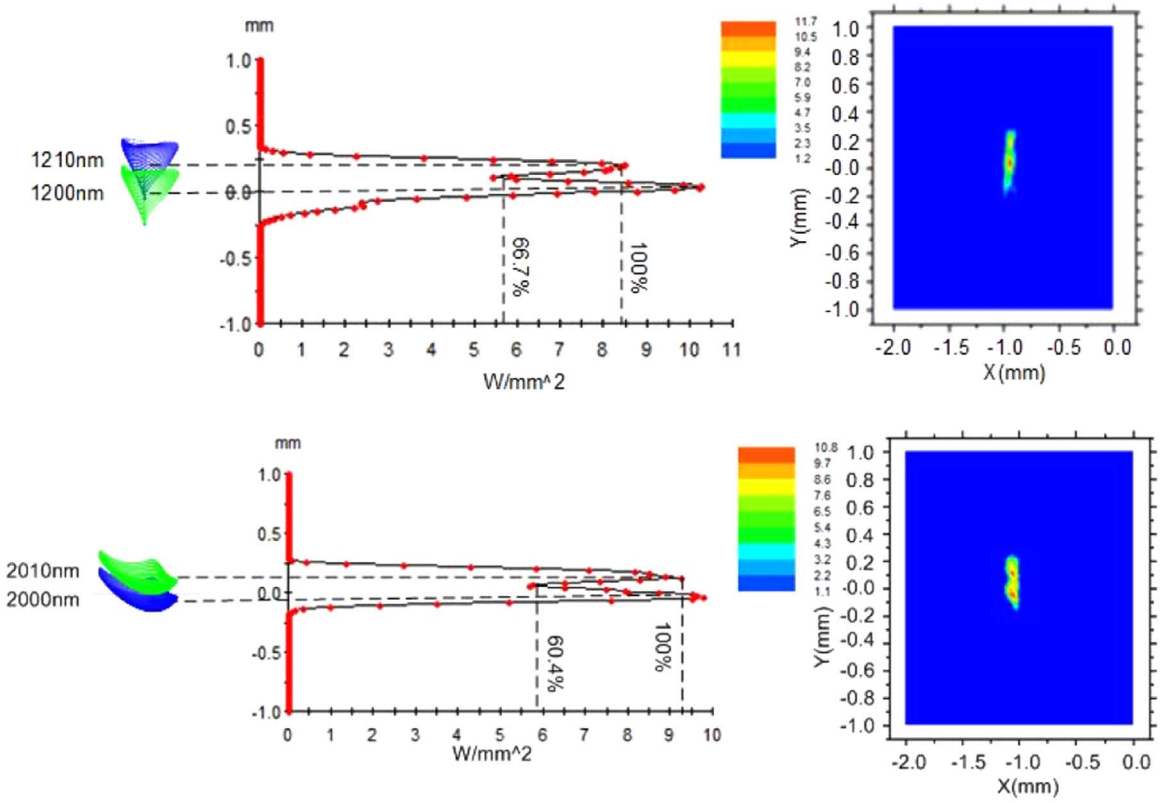

Fig. 9. Spot diagrams of the fiber's image and the corresponding energy distribution and irradiance chart on DMD.

the two sets of wavelengths on DMD can be distinguished, and the simulated resolution is better than 10 nm. The total size of the optical system is about 80 mm × 65 mm × 30 mm.

In our previous spectrometer [5], three pieces of lenses and two sub-gratings are needed to fold the spectra on DMD. The only way to increase the number of the spectra folds is to increase the number of sub-gratings, which may cause much more energy absorbed by grating holders and lead to larger error during the alignment as well. Fig. 10(a) and (b) shows the energy absorbed by two grating holder is about 11.5% of the source energy, and the irradiance maps are obtained by setting the grating holder as perfect absorber. The flux for the zero order diffraction and the second order diffraction of the two sub-gratings is about 16.7% of the source energy. However, in the spectrometer we designed above, one freeform lens and one plane grating can achieve the spectra folding perfectly, which makes the spectrometer more compact than before. And only the freeform lens needs to be redesigned when the number of the spectral folds increases. The energy loss caused by the dislocation on the freeform surface is 0.23%, as shown in Fig. 10(c), and the irradiance map is obtained by placing a perfect absorber behind the lens. The flux for the zero order and the second order diffraction light of the plane grating is about 13.1% of the source energy. The stray light caused by the sag departure of the freeform surface can be eliminated by coating a stripe absorbing film (with a width of 180 μm) on the spherical surface along the direction of the dislocation, and the absorbed energy is about 1.22% of the source energy. Table 1 shows the energy and structure comparison between the two kinds of Hadamard Transform spectrometers. If the freeform lens is volume-produced by injection molding method, the cost will be quite low. So it is prospective to be used in many commercial applications where high resolution and wide working wavelength range are required at the same time.

Considering that the broadband spectra from the source propagate through both the upper and lower parts of the freeform

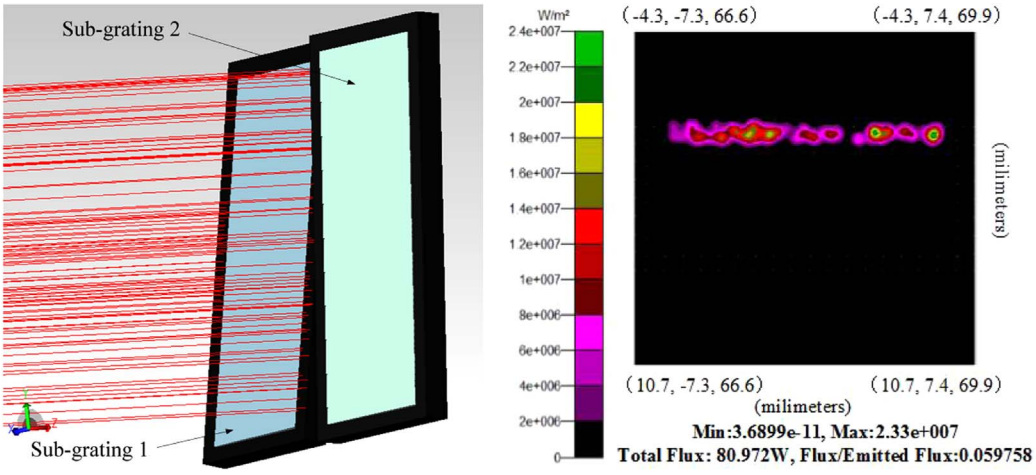

(a) Energy absorbed by grating holder of sub-grating 1 and the irradiance map on the grating holder.

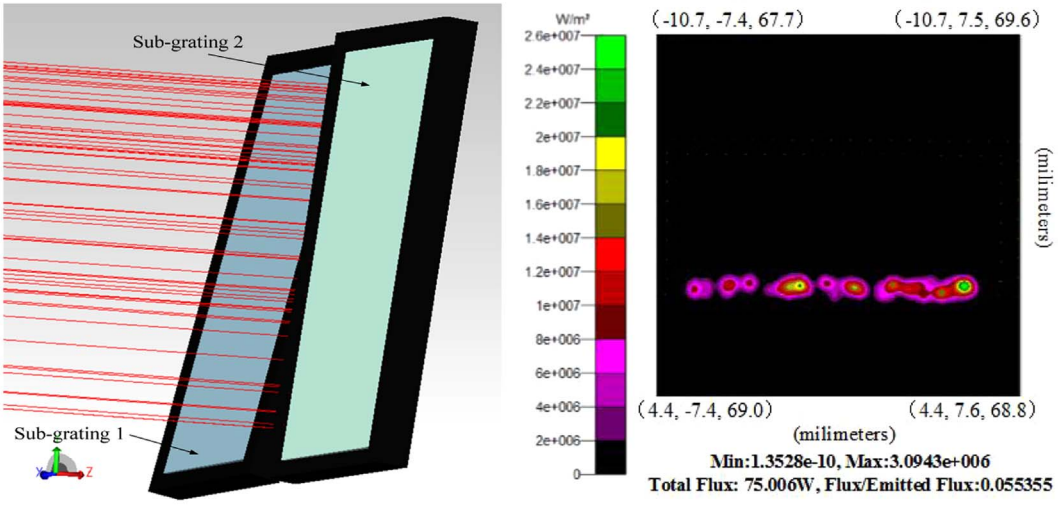

(b) Energy absorbed by grating holder of sub-grating 2 and the irradiance map on the grating holder.

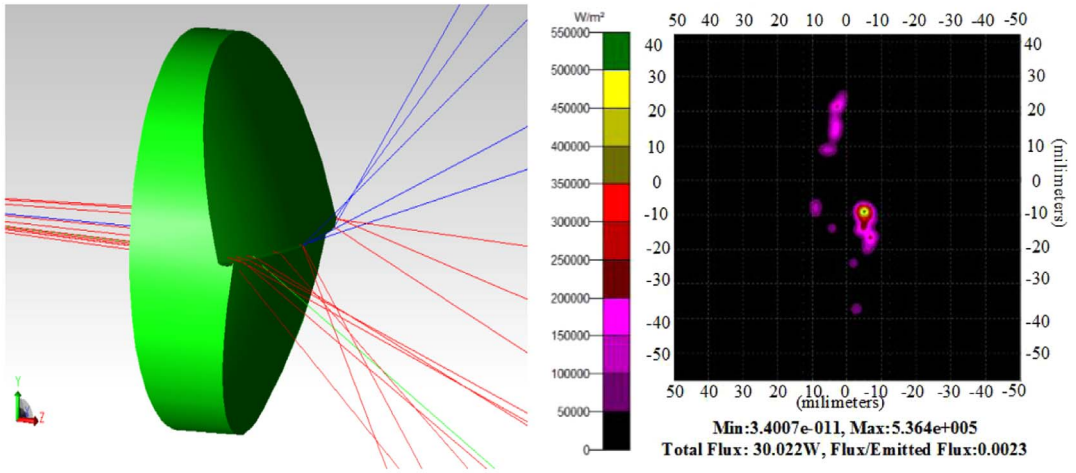

(c) Energy loss caused by the dislocation on the freeform surface and the irradiance map on perfect absorber.

Fig. 10. Comparison of sub-gratings and the freeform lens in the two kinds of HTS.

Table 1
Comparison of the two kinds of HTS.

	Freeform lens collimated HTS	Sub-grating HTS
Elements to achieve spectra fold	One freeform lens, one grating	Three piece of lenses, two sub-gratings
Energy loss (respect to source energy)	14.32%	26.3%

lens, measures should be taken to suppress the stray light. Given that the secondary spectrum of 800 nm will overlap with 1600 nm, two band-pass filters with pass-band from 800 nm to 1580 nm and 1580 nm to 2400 nm are placed behind the corresponding parts of the freeform lens to block the wavelengths from 1580 nm to 2400 nm and 800 nm to 1580 nm. Meanwhile, the spectra from 1580 nm to 2400 nm will not be influenced by the secondary spectra of 800 nm to 1200 nm, which is another advantage of the spectrum-folded spectrometer compared with traditional broadband spectrometers.

4. Conclusion

In this study, a novel Hadamard transform spectrometer collimated by a freeform lens is designed which doubles the spectral bandwidth while maintaining the resolution. The freeform lens redistributes the light beam of source into two collimated beams with different wavelengths and different angles. The entire spectral band from 800 nm to 2500 nm is folded on DMD as two parallel and aligned spectra bands, from 800 nm to 1600 nm and from 1600 nm to 2400 nm. The simulation results show that the spectral resolution is 10 nm, and the diffraction efficiency of the grating becomes more uniform. Compared with the prior spectrometer we designed, the optical system of this spectrometer becomes more compact, and the energy efficiency is improved by 11.98%. Further work will focus on the design of freeform surfaces which can collimate the broadband spectra irradiant from extended light sources.

Acknowledgment

The authors appreciate the support of the Innovation of Science and Technology in Jilin Province youth leading talent and team project (Grant no. 20160519021JH).

References

[1] Y. Ozaki, W. Fred Mcclure, A.A. Christy. Near-infrared Spectroscopy in Food Science and Technology [M]. Wiley Interscience, A John Wiley & Sons, Inc., Publication, 2007.
[2] Marcelo Blanco, Anna Peguero, Analysis of pharmaceuticals by NIR spectroscopy without a reference method, Trends Anal. Chem. 29 (10) (2010) 1128–1136.
[3] H.M. Heise, R. Marbach, A. Bittner, et al., Clinical chemistry and near infrared spectroscopy: multicomponent assay for human plasma and its evaluation for the determination of blood substrates, J. Infrared Spectrosc. 6 (1998) 361–374.
[4] J. Wu, S. Zhu, Y. Xu, et al., Study on detection technology vector machines and near infrared of milk powder based on support spectroscopy, IFIP Int. Fed. Inf. Process. (2008) 259.
[5] X. Wang, H. Liu, Z. Lu, L. Song, T. Wang, B. Dang, X. Quan, Y. Li, Design of a spectrum-folded Hadamard transform spectrometer in near-infrared band, Opt. Commun. 333 (2014) 80–83.
[6] Minghui Liu, Suxing Pan, Yuerui Chen, et al., Path-folded infrared spectrometer consisting of 10 sub-gratings and a two-dimensional InGaAs detector, Opt. Express 17 (17) (2009) 14956–14966.
[7] A. Bruneton, A. Baeuerle, R. Wester, J. Stollenwerk, P. Loosen, High resolution irradiance tailoring using multiple freeform surfaces, Opt. Express 21 (9) (2013) 10563–10571.
[8] A. Bauerle, A. Bruneton, R. Wester, J. Stollenwerk, P. Loosen, Algorithm for irradiance tailoring using multiple freeform optical surfaces, Opt. Express 20 (2012) 14477–14485.
[9] Z. Feng, L. Huang, M. Gong, G. Jin, Beam shaping system design using double freeform optical surfaces, Opt. Express 21 (12) (2013) 14728–14735.
[10] Juan C. Minano, Pablo Benitez, Asuncion Santamaria, Free-form optics for illumination, Opt. Rev. 16 (2) (2009) 99–102.
[11] M. Hanf, R. Hahn, W. Dotzel, T. Gessner, A dynamically driven micro mirror array as the encoding mask in a Hadamard transform spectrometer (HTS), Sens. Actuators A 123–124 (2005) 476–482.
[12] B.K. Harms, J.B. Park, S.A. Dyer, On the use of fast Hadamard transforms for spectrum recovery in Hadamard transform spectroscopy, Appl. Spectrosc. 46 (9) (1992) 1358–1361.
[13] A. Bruneton, A. Baeuerle, R. Wester, J. Stollenwerk, P. Loosen, Limitation of the ray mapping approach in freeform optics design, Opt. Lett. 38 (11) (2013) 1945–1947.
[14] Y. Ding, X. Liu, Z.R. Zheng, P.F. Gu, Freeform LED lens for uniform illumination, Opt. Express 6 (17) (2008) 12958–12966.
[15] L. Wang, K.Y. Qian, Y. Luo, Discontinuous free-form lens design for prescribed irradiance, Appl. Opt. 46 (18) (2007) 3716–3723.
[16] F.Z. Fang, Y.H. Chen, X.D. Zhang, X.T. Hu, G.X. Zhang, Nanometric cutting of single crystal silicon surfaces modified by ion implantation, CIRP Ann.-Manuf. Technol. 60 (1) (2011) 527–530.
[17] W. Michaeli, S. Hessner, F. Klaiber, J. Forster, Geometrical accuracy and optical performance of injection moulded and injection-compression moulded plastic parts, Ann. CIRP 56 (1) (2007) 545–548.